New insights into the anomaly genesis of frequency selection method: supported by numerical modeling and case studies

Tian Chun Yang
Hunan University of Science and Technology
Qiang Shan Gao (gaoqiangshan@nssc.ac.cn)
Chinese Academy of Sciences
Hao Li
State Key Laboratory of Gas Disaster Detecting, Preventing and Emergency Controlling
Guo Hong Fu
Hunan University of Science and Technology
Yawar Hussain
University of Liege

Research Article

Keywords: Profile curve, Pseudo-sections, noodles phenomenon, Geophysics, Frequency selection method of telluric current (FSM), Groundwater, Magnetotelluric sounding (MT)

Posted Date: July 15th, 2022

DOI: https://doi.org/10.21203/rs.3.rs-1854503/v1

New insights into the anomaly genesis of frequency selection method: supported by numerical modeling and case studies

TianChun YANG [1], QiangShan GAO[2*], Hao LI [3], GuoHong FU [1], Yawar HUSSAIN[4]

1 School of Earth Sciences and Spatial Information Engineering, Hunan University of Science and Technology, Xiangtan 411201, China

2. State Key Laboratory of Space Weather, National Space Science Center, Chinese Academy of Sciences, Beijing 100190, China

3. State Key Laboratory of Gas Disaster Detecting, Preventing and Emergency Controlling, Chongqing 400037, China

4. Georisk & Environment, Department of Geology, University of Liege, Liege, 4000, Belgium

Abstract: The frequency selection method (FSM) is the further development of audio frequency telluric electricity method (TEFM), however there are still ongoing debates on the involving mechanisms leading to anomaly genesis. Therefore, the present study intends to explore this using 2D forward modeling of magnetotelluric (MT) sounding, and practical applications of FSM on three Chinese case studies in karst and granitic settings. In the first stage, the profile curves and pseudo-section of apparent resistivity (ρ_s) and horizontal electric field component (E_y) in Transverse Magnetic field （TM） mode are obtained by forward calculation. As a result, the static shift in ρ_s is observed over the near-surface inhomogeneities, as documented in literature. Additionally, the profile curves of E_y showed an obvious static shift in the rectangular coordinate system (i.e., the curve rises with the increase in frequency) which is a well-known phenomenon. The pseudo-sections of E_y also showed static shift characteristics at the horizontal position above the anomaly, referred to as "noodles phenomenon". The FSM results obtained from case studies related to the groundwater and low resistivity clay-filled karst body identification. The ΔV section curves and pseudo-section showed a significant low potential, and a "noodles phenomenon" respectively, above the low resistive anomalous body. These abnormal characteristics of ΔV are the basis for delineating the horizontal position of groundwater aquifer applying FSM. It is concluded that the anomaly of FSM is the reflection of the static shift in MT and hence, the FSM can be categorized as a "static shift method". Therefore, this inspired us that the static shift feature of surface E_y component can be utilized to explore near-surface geological bodies such as clay-filled or water-filled cavities.

Keywords： Profile curve; Pseudo-sections; noodles phenomenon; Geophysics; Frequency selection method of telluric current (FSM); Groundwater; Magnetotelluric sounding (MT)

0 Introduction

The frequency selection method (FSM) is a general name given to numerous similar methods proposed by Chinese scholars in the early 1980s successively, such as electric pulse method of natural field, stray current method (or audio earth potential method), the frequency selection method of telluric current, sound frequency geoelectric field method, natural low-frequency electric field method, geoelectric frequency selection method, audio frequency telluric electricity method, interference electric field method, natural alternating field method, underground magnetic fluid detection method. These methods work on the same detection principle and measuring methods of equipment and are therefore generally called FSM. FSM is naturally the further development and application of audio frequency telluric electricity method (TEFM). The field operations of FSM and AMT (audio magnetotelluric method) are the same; however, FSM measures the horizontal components of the electric field at different frequencies of electromagnetic signals in the earth surface.

At present, the advancement in geophysical instrumentation has expanded the working frequencies to the range of 10 ~ 5000 Hz. The potential electrode spacing is usually set at 10 or 20 meters as an implementing section method. Therefore, the instruments have the advantages of being portable type, simple operation, and high efficiency. Since the 1980s, the development of FSM including instrumentation and applications has been in a flourishing state. B. H. Liang proposed the electric pulse of the natural field method in 1976 and applied it to explore the groundwater (Yang

* Corresponding author

E-mail address：gaoqiangshan@nssc.ac.cn(Gao Q. S.), ytc6803@163.com (Yang T. C.)

1982). Yang (1982) proposed the stray current method and carried out theoretical research on the basis of experiments. Xin (1982) proposed the audio geoelectric field method and the relative SDD-1 acoustic geodetic field instruments had been further popularized. Lin et al. (1983) proposed a natural low-frequency electric field method and modeled the distribution law of the anomaly of frequency selection on the vertical dike model according to the propagation law of magnetotelluric electromagnetic field. Han and Wu (1985) proposed a frequency selection method for the telluric electricity field and developed the DX-1 frequency selection instrument for the telluric electricity field by referencing the magnetotelluric instrument. Their instrument had been well promoted and applied in China in the past. Recently, Han and Han (2020) compiled their practical application examples over years into a monograph. Bao (1994) proposed the interfering electric field method and developed the corresponding instrument, implementing indoor simulation experiments and a considerable number of field measurements. Zhou et al. (2009) proposed an underground magneto fluid detecting method and developed an underground magneto fluid detector and portable underground water source detector. Some other geologists mentioned some other name concepts in their published articles (Luo, 1994; Liang et al., 2016). The FSM has already acquired successful applications in the exploration of shallow groundwater resources, and hazards associated with mine water (Farzamian et al., 2019; Yang et al., 2020a; Yang et al., 2020b; Song et al., 2021; Singh et al., 2022). However, the nature of these concepts still belongs to FSM according to the equipment they used.

Since its introduction, numerous studies have been carried out with the main focus on the development and application of instruments, especially in groundwater resources and disaster studies, using various types of instruments. Nevertheless, there is limited theoretical research on this method. One possible reason is the complexity of natural sources, and factors of human structures making the measurement of shallow natural electromagnetic source fields challenging. Additionally, the manual reading from the instrument was complicated before the advent of an intelligent frequency selector. The electric field components measured by the pointer-deflecting instrument are only a few limited frequencies that inhibit the profile curve understanding. Yang et al. (2017 & 2020a) focused more on the theoretical research of FSM and completed some relevant studies driven by long-term practical applications. Though some simple relative geological models can simulate the abnormal curves similar to the real ones, many aspects of FSM studies, such as the size and ranges of the anomaly, seem to achieve unsatisfactory results.

MT is a passive source electromagnetic method with a field source, proposed by A. N. Tikllonov and L. Cagnird in the early 1950s. MT, due to its great exploration depth, has been widely applied to oil and gas fields, coal mines, metal mines, karst water structure, crustal lithosphere structure, and other aspects (Yang et al., 2019). The MT forward can be realized by the integral equation method, finite difference, or finite element method, and the numerical solution is obtained by the approximation of differential or integral equation and the solution of linear equations. The finite element method is more advantageous in MT forward calculation than the other two methods. Coggon (1971) firstly realized the importance of electromagnetic forward simulation of finite element methods. Subsequently, some experts applied the MT forward by using rectangular elements, triangular elements, mixed elements, and unstructured triangulation elements, respectively. Chen (1981) and Hu et al. (1982) implemented MT forward modeling research. Xu (1994) further studied the finite element and mesh portioning. Chen et al. (2000) proposed the finite element direct iteration algorithm. Tan et al. (2003) introduced the biconjugate stable gradient method based on previous studies. Zhou et al. (2021) studied forward and inversion of 2.5-D electromagnetic methods in the frequency domain. After years of in-depth research, 2D and 3D finite element forward electromagnetic methods have attained some stability and become one of the significant means to study electromagnetic issues.

The static shift is unavoidable in magnetotelluric observation which is often confused with interference and so suppressed or eliminated especially in deep target studies (Di et al., 2019; Hu et al., 2017; Xiong et al., 2021). Just as in the initial period of seismic exploration, Rayleigh waves were always treated as interference signals (Yang and He, 2013). Meanwhile, many studies have been carried out on the formation mechanism of static shift and its relationship with the presence of shallow anomalous bodies. Liu et al. (2018) also presented one viewpoint of using static excursion distortion law to detect the shallow anomalous body. According to the propagation feature of electromagnetic fields in the horizontal uniform layered medium, the direction of the current field is parallel to the interface having no accumulated charge. However, the charges can be accumulated on the interface where the presence of the surface or subsurface single inhomogeneous body can cause distortions in the observed electric field on the surface (Figure 1). Similarly, the MT sounding curve will also have a static shift, attributed to the low frequency characteristics of the magnetotelluric field. In the case where the scale of electrical inhomogeneity is much larger than the wavelength of electromagnetic waves, the observed changes in apparent resistivity curve and phase curve are not considered as static shift (Huang et al., 2006).

This paper discusses the main causes of abnormal results obtained from the frequency selection telluric current method (FSM) based on the causes and features of the static shift of the magnetotelluric (MT) sounding. The objectives are achieved by simulating the static shift of MT using the finite element method based on Maxwell's equation. Unlike previous studies only considering the static shift feature of apparent resistivity and phase curves, we further focused on analyzing the characteristics of surface electric field components. Additionally, three case studies on karst and granitic geological settings have been considered for the validation of numerical findings. The outcomes of the present study will improve future applications of FSM through a better understanding of the physical nature.

1 Basic theory

1.1 Cause of static shift

The interface will accumulate charge when the current flows through the interface of an inhomogeneous body. According to Gauss law, continuity equation of current and approximation under quasi-static condition, we can deduce the surface charge density q_s on the conductive medium surface as follow

$$q_s = E_{n2}\varepsilon_0 \frac{\sigma_2-\sigma_1}{\sigma_1} = E_{n1}\varepsilon_0 \frac{\sigma_2-\sigma_1}{\sigma_2} \quad (1)$$

Where

σ_1 and σ_2 are the conductivity of the inhomogeneous body and the surrounding rock respectively,

E_{n1} and E_{n2} are the strength of normal electric field at the interface of the body and rock,

ε_0 is the dielectric constant.

Though q_s is small for the field, its effect on the electric field is negligible, which is the physical cause of the static displacement. The influence of accumulated charge on the surface can be detected by the instrument when the skin depth is much larger than the size of the inhomogeneous body, e.g. the situation shown as figure 1. MT is always affected by the small inhomogeneous body at the surface or subsurface as exploring deep geological bodies. According to previous research, the secondary electric field generated by the accumulated charge has a positive relationship with the same phase of the primary field, being independent of frequency at the same time. Only Transverse Magnetic field (TM) mode is affected under strict two-dimension geological conditions, while both TM and Transverse Electric field (TE) mode are affected in three-dimension condition. In addition, the static displacement is also related to underground resistivity, position of electric field electrode, length of electric measuring dipole and size ratio of the inhomogeneous body.

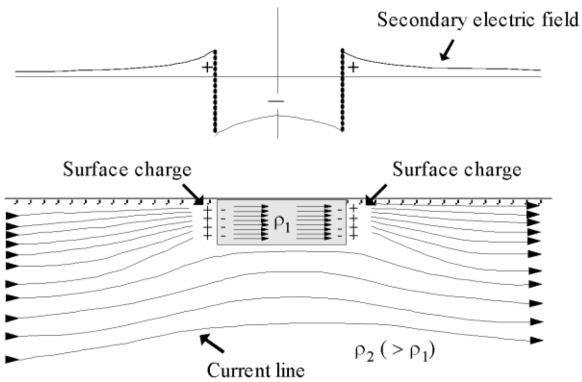

Figure 1 A schematic diagram of TM mode electric field response of a near surface low resistivity anomaly (adopted after Liu et al., 2018).

1.2 2D forward modeling theory of MT

1.2.1 Boundary and variational problem

Any electromagnetic problems can satisfy Maxwell equations. The forward simulation studies a steady state field problem under the conditions satisfied by natural electromagnetic method. Given that the angular frequency is ω, the time-dependence is $e^{-\mathrm{i}\omega t}$, MT responses can be described by Maxwell's equations

$$\nabla \times \boldsymbol{E} = \mathrm{i}\omega\mu\boldsymbol{H} \tag{2}$$

$$\nabla \times \boldsymbol{H} = (\sigma - \mathrm{i}\omega\varepsilon)\boldsymbol{E} \tag{3}$$

Where

E and H are electric and magnetic fields respectively,

μ, σ and ε are magnetic permeability, electrical conductivity and permittivity respectively,

i is imaginary unit and $i^2 = -1$.

Given that the underground electrical structure is two dimensional and the strike is along x axis, y axis is perpendicular to x axis and horizontally to the right, z axis is vertically downward (Figure 2). As the electromagnetic field propagates vertically downward into the medium in the form of plane waves, Eq. (2) and (3) are expanded according to components, two independent polarization modes (TE and TM) can be obtained. Since FSM generally only measures the horizontal electric field component along the survey line, this study only discusses the TM polarization mode. The equations in the TM mode are as follow

$$\frac{\partial E_z}{\partial y} - \frac{\partial E_y}{\partial z} = \mathrm{i}\omega\mu H_x\,, \quad E_y = \frac{1}{\sigma - \mathrm{i}\omega\varepsilon}\frac{\partial H_x}{\partial z}, \quad E_z = \frac{-1}{\sigma - \mathrm{i}\omega\varepsilon}\frac{\partial H_x}{\partial y} \tag{4}$$

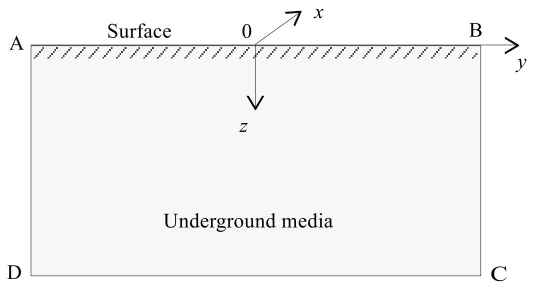

Figure 2 studied the area of TM polarization mode for MT.

where H_x in Eq. (4) satisfies the following partial differential equation.

$$\frac{\partial}{\partial y}\left(\frac{1}{\sigma - \mathrm{i}\omega\varepsilon}\frac{\partial H_x}{\partial y}\right) + \frac{\partial}{\partial z}\left(\frac{1}{\sigma - \mathrm{i}\omega\varepsilon}\frac{\partial H_x}{\partial z}\right) + \mathrm{i}\omega\mu H_x = 0 \tag{5}$$

Let if $u = H_x$, $\tau = \frac{1}{(\sigma - \mathrm{i}\omega\varepsilon)}$, $\lambda = \mathrm{i}\omega\mu$, the variational problem corresponding to 2D MT forward modeling solved by the finite element method is as follow

$$F(u) = \int_{\Omega} \left[\frac{1}{2}\tau(\nabla u)^2 - \frac{1}{2}\lambda u^2\right] d\Omega + \int_{\mathrm{CD}} \frac{1}{2}\tau k u^2\, d\Gamma, \quad u|_{AB} = 1, \quad \delta F(u) = 0 \tag{6}$$

Where

Ω represents whole computational domain,

AB and CD are respectively upper and lower bounds in Figure 2,

k is wave number and $k = \sqrt{-\mathrm{i}\omega\mu\sigma - \omega^2\mu\varepsilon}$, or $k = \sqrt{-\mathrm{i}\omega\mu\sigma}$ if the displacement current neglected.

1.2.2 2D finite element method

In order to improve the accuracy of simulation, the computational domain is discretized as rectangular elements. Biquadratic interpolation is adopted in this rectangular element, namely, each element takes a total of eight points at the four vertices and four midpoints of the four edges. Through the unit analysis of unit e, the unit integrals of the three integrals in the first equation in Eq. (6) can be separated into

$$\int_e \frac{1}{2}\tau(\nabla u)^2\, d\Omega = \frac{1}{2}\boldsymbol{u}_e^{\mathrm{T}}(k_{ij})\boldsymbol{u}_e = \frac{1}{2}\boldsymbol{u}_e^{\mathrm{T}}\boldsymbol{K}_{1e}\boldsymbol{u}_e \tag{7}$$

$$\int_e \frac{1}{2}\lambda u^2\, d\Omega = \frac{1}{2}\boldsymbol{u}_e^{\mathrm{T}}(k_{ij})\boldsymbol{u}_e = \frac{1}{2}\boldsymbol{u}_e^{\mathrm{T}}\boldsymbol{K}_{2e}\boldsymbol{u}_e \tag{8}$$

$$\int_{\mathrm{CD}} \frac{1}{2}\tau k u^2 d\Gamma = \frac{1}{2}\boldsymbol{u}_e^{\mathrm{T}}(k_{ij})\boldsymbol{u}_e = \frac{1}{2}\boldsymbol{u}_e^{\mathrm{T}}\boldsymbol{K}_{3e}\boldsymbol{u}_e \tag{9}$$

In the above equations, T represents transposition of the matrix. The specific formulas of coefficient matrices $\boldsymbol{K}_{1e}$, $\boldsymbol{K}_{2e}$ and $\boldsymbol{K}_{3e}$ can be found from Xu (1994) and Liu et al. (2009).

Extend $\boldsymbol{K}_{1e}$, $\boldsymbol{K}_{2e}$ and $\boldsymbol{K}_{3e}$ into a matrix composed of all nodes, that is, sum all elements and get

$$F(u)=\sum F_e(u)=\sum \frac{1}{2}\boldsymbol{u}_e^T(\boldsymbol{K}_{1e}-\boldsymbol{K}_{2e}+\boldsymbol{K}_{3e})\boldsymbol{u}_e=\frac{1}{2}\boldsymbol{u}^T\sum \boldsymbol{K}_e\,\boldsymbol{u}=\frac{1}{2}\boldsymbol{u}^T\boldsymbol{K}\boldsymbol{u} \qquad (10)$$

By taking the Eq. (10) and making it equal to zero, a system of linear equations can be obtained as follow

$$\boldsymbol{K}\boldsymbol{u}=0 \qquad (11)$$

where $\boldsymbol{K}$ is an overall stiffness matrix. Then, the solution of the linear equations namely u of each node can be obtained by substituting the upper boundary value of Eq. (6).

After calculating the u value of each node (i.e. H_x of TM polarization mode), we can solve the partial derivative of $\frac{\partial u}{\partial z}$ along the vertical direction of the surface by using the difference method.

$$\left.\frac{\partial H_x}{\partial z}\right|_{z=0}=\frac{1}{2l}(-11H_{x1}+18H_{x2}-9H_{x3}+2H_{x4}) \qquad (12)$$

where

H_{x1} represents the field value of surface,

H_{x2}, H_{x3} and H_{x4} are the field values at the first three isometric grid nodes below the surface respectively,

l is the vertical distance from the first node to the four node.

At last, the E_y value can be calculated by the second formula in the Eq. (4) along the horizontal direction. Meanwhile, the impedance Z_{TM}, the apparent resistivity ρ_a^{TM} and the impedance phase φ^{TM} of TM polarization mode can be calculated by the following formulas.

$$Z_{\mathrm{TM}}=\left(\frac{1}{\sigma-\mathrm{i}\omega\varepsilon}\frac{\partial H_x}{\partial z}\right)/H_x\approx\left(\frac{1}{\sigma}\frac{\partial H_x}{\partial z}\right)/H_x,\quad \rho_a^{\mathrm{TM}}=\frac{1}{\omega\mu}|Z_{\mathrm{TM}}|^2,\quad \varphi^{\mathrm{TM}}=\arctan\frac{\mathrm{Im}[Z_{\mathrm{TM}}]}{\mathrm{Re}[Z_{\mathrm{TM}}]} \qquad (13)$$

1.2.3 Solution of linear equations and mesh generation

Two dimensional finite element forward calculation of MT ultimately comes down to solving symmetric large-scale spare and ill-posed linear equations with complex coefficients. The $\boldsymbol{K}$ in Eq. (11) is positive definite. These equations can be solved by many methods such as singular values decomposition, the Newton method, conjugate gradient (CG) method, etc. This study adopted the BICGSTAB algorithm without completely LU decomposition, which has advantages of fast, high precision and good stability.

Only the non-zero elements of the sparse matrix are stored in the solving process. In addition, the square grid can decrease the error of calculation near the boundary through the trail calculation of the uniform half-space model. Therefore, we use the square grid as much as possible to expand the modeling calculation area on the premise of ensuring the calculation accuracy and fully utilizing the storage space of the computer.

2 Numerical analysis

Applying the aforementioned 2D finite element simulation theory of MT, we can carry out the forward calculation using 2D geological geophysical models. A forward model of two layered horizontal stratified medium with one caly-filled karst anomaly in the substrate layer was chosen (Figure 3). The entire computational domain constitutes an area of 6 × 3 km^2 and discretized into 120 × 60 = 7200, namely AB is 6 km and AD is 3 km. The grid size (d_y and d_z) of simulation is fixed as 50m and fifty three frequencies are used (f =10.^(-4:0.125:2.5) Hz).

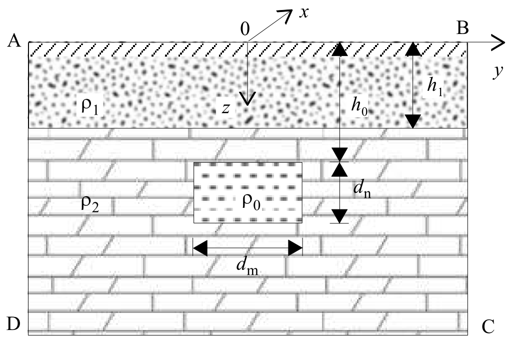

Figure 3 An abnormal body in layered half space of model 1. The upper layer represents fine loose sediment with attributed resistivity value of 150 Ω·m, while the substrate layer is the dolomitic limestone with resistivity 2200 Ω·m. One low resistivitive clay-filled karst body is introduced in the model.

Figure 4 shows the results of the model 1 in terms of ρ_s and E_y, and their corresponding pseudo sections. For convenience, only the results of three frequencies (1 Hz, 10 Hz and 100 Hz) are drawn in Figure 4a, which reflects a downward shifts in the ρ_s curve with the increase in frequency, a typical characteristic of static shift. The E_y profile curves in Figure 4b display good differentiation in the Cartesian coordinate system, and their curve forms at the three frequencies remained unchanged, rising significantly with the increase of frequency. Meanwhile, the relative low potential anomaly directly above the abnormal body also increased significantly.

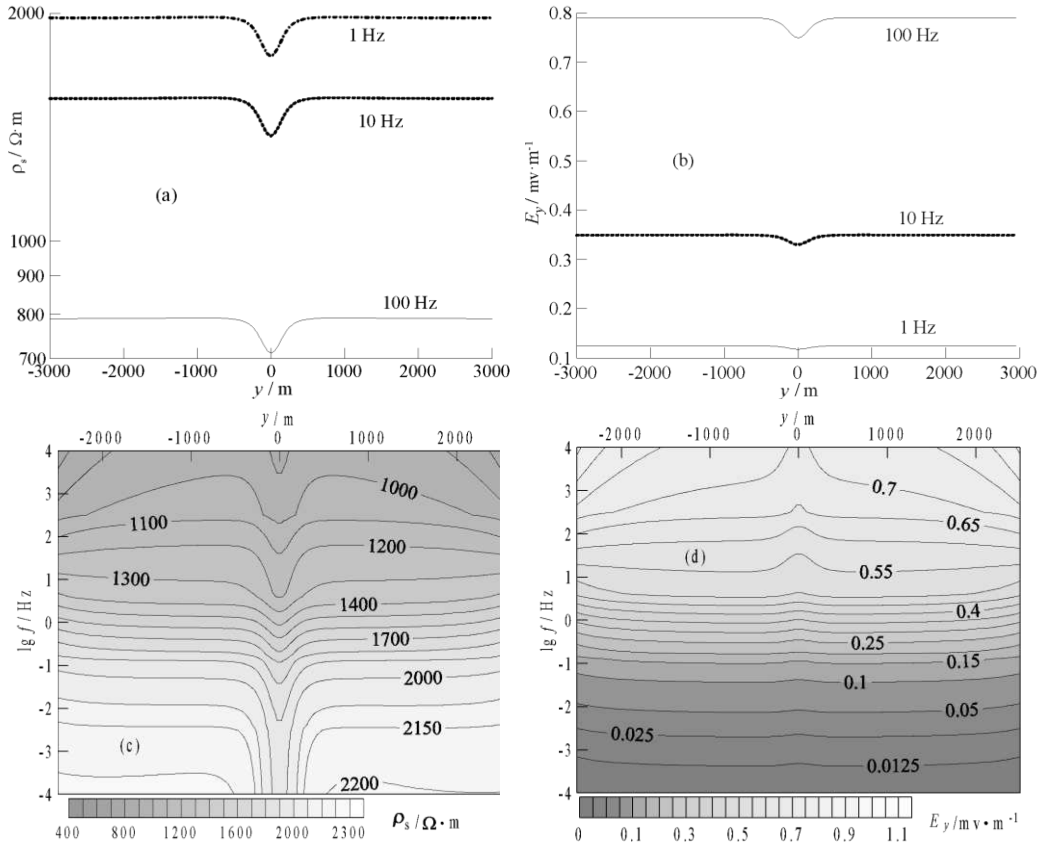

Figure 4 The results of model 1. (a) Curves of apparent resistivity ρ_s, the vertical axis is logarithmic coordinate; (b) Curves of horizontal electric field component E_y; (c) Pseudo section of ρ_s; (d) Pseudo section of E_y.

Figure 4c shows the obvious "noodles phenomenon" (or “hanging noodles phenomenon”) caused by the static shift. The ρ_s isoline stretches downward at the position corresponding to the abnormal body. The lower the frequency is, the more obvious the stretching is. This phenomenon has been documented in the literature, expected to be eliminated or suppressed in the measured data of MT, CSAMT and wide field electromagnetic method (WFEM) (Tournerie et al., 2007; Lei et al., 2017; Li and He, 2021). The pseudo section of E_y component in Figure 4d also shows the similar phenomenon, but the stretching direction of isoline is upward and becomes more obvious with the increase in frequency. At the same time, the magnitude of the anomaly is not so obvious as the ρ_s isoline.

In the FSM application, the frequencies are mostly selected in the audio range. Compared with MT, the overall working frequencies of FSM are higher, for example, the frequencies of the pointer DX-1 type frequency selector are set only five, namely 14.6 Hz, 71.8 Hz, 161 Hz, 262 Hz, 327 Hz and 783 Hz, and the intelligent PQWT-TC300 operates at forty frequencies in the range of 12 ~ 5000 Hz. For another, the main exploration targets of the selector are the relatively shallow media, for instance, the apparent depth of PQWT-TC150 and TC300 inversion is 150 m and 300 m respectively.

In addition, the size of the target body detected by FSM is generally relatively small. Target of most underground exploration in karst environment is either fissure, fault or other geological structures. The size of them is generally not as large as that of the model 1 (Figure 3). Therefore, another shallow buried water channel model is adopted and discussed as under.

The next model is a water channel model constituting a horizontal two-layer, upper loose sediment and substrate granite layer. The water channel is supposed to be in the upper layer, semi-filled with air and water. The entire computational domain ABCD is 50 × 30 m^2 and discretized into 100 × 60 = 6000, having a grid size of 0.5 m (Figure 5). The calculated frequencies are 40 frequencies in the 12 ~ 5000 Hz range, same as can be detected by the TC300 frequency selector instrument.

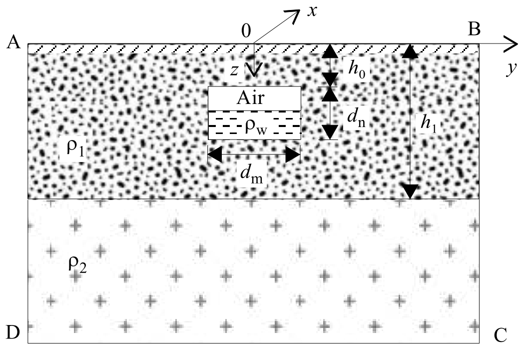

Figure 5 Water channel of model 2. The upper layer represents fine loose sediment (150 Ω·m) while substrate is granite (2200 Ω·m).

The results of model 2 are shown in Figure 6 which are similar with those presented in Figure 4. The FSM often uses three frequencies (25 Hz, 67 Hz and 170 Hz) to scan underground section, the respective ρ_s profile curves of these three frequencies (Figure 6a) are quite similar to the curves of model 1, as shift downward with the increase in frequency, but the waveform of curves remains unaffected. The static shift in Figure 6b ~ 6d is still very obvious, and the "noodles phenomenon" is more prominent. The profile curve shows a local maximum at y=0, which may be the result of the high resistance (i.e., air) filling the upper part of the channel. The ordinate in Figure 6c and 6d is the pseudo-depth of approximate inversion based on the skin depth formula of electromagnetic waves, the pseudo-depth is the same as that of the real-time result inversion method adopted by the field instrument.

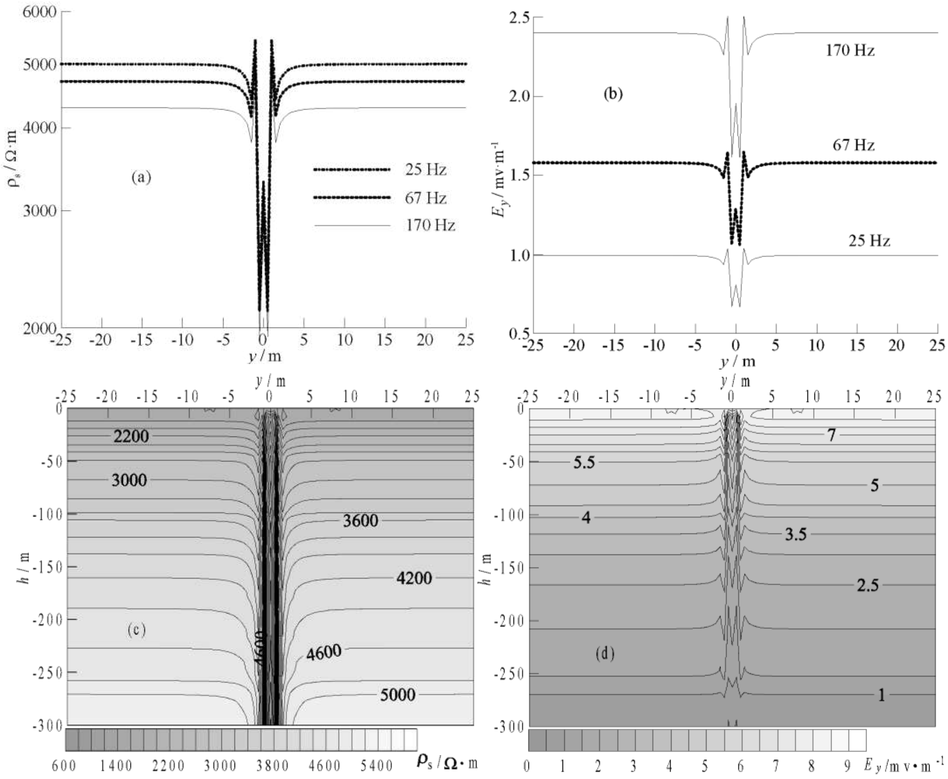

Figure 6 Results of the model 2 with (a) curves of apparent resistivity ρ_s; (b) curves of horizontal electric field component E_y; (c) pseudo section of ρ_s; (d) pseudo section of E_y.

It is can be concluded from the two considered theoretical models that the static shift in the horizontal electric field component E_y profile curve generated by the natural electromagnetic field at the surface is an obvious phenomenon in the Cartesian coordinate system, but the relationship between the lifting direction of the profile curve and the frequency is opposite to that of the ρ_s profile curve. Meanwhile, the static shift is still obvious in the E_y pseudo profile, but the stretching direction of E_y isoline is opposite to that of ρ_s. The static shifts of ρ_s and E_y curves are all caused by the presence of near-surface inhomogeneity. Therefore, this inspired us that the static shift feature of surface E_y component can be utilized to explore near-surface geological bodies such as clay-filled or water-filled cavities.

3 Case studies

Three perspective sites in the karst and granitic environments are chosen using different instruments capable of measuring different frequencies ranges for the comparison purpose with the numerical findings.

In accordance with the case studies on the application of FSM, the present study applied the method using three frequencies in data acquisition in Lengshuijiang City (27°40'45"N and 111°26'27"E). Geologically, the considered region is carboniferous limestone exposed on the surface. Data were acquired using TC300 equipment with electrode spacing (MN) and station interval as 10 m and 5 m, respectively. The drilling position was set at 15 m from the start of the profile represented as black point in Figure 7. The water flow rate was about 100 t/day drilled at 100 m depth while at 150 m depth water yield exceeded 300 t/day. The main outlet depth is about 120 m. Figure 7 is the curve chart of measured results of the FSM at three frequencies in Lengshuijiang City (Figure 8), Hunan Province, China. Due to only a few frequencies being observed at that time, it is difficult to clearly recognize the cause of the anomaly from these curves.

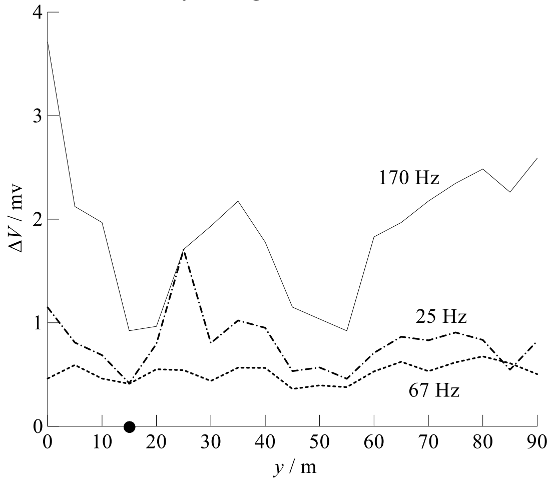

Figure 7 Profile exploration results of FSM in Lengshuijiang City. The black point marks the drilling position for water exploration.

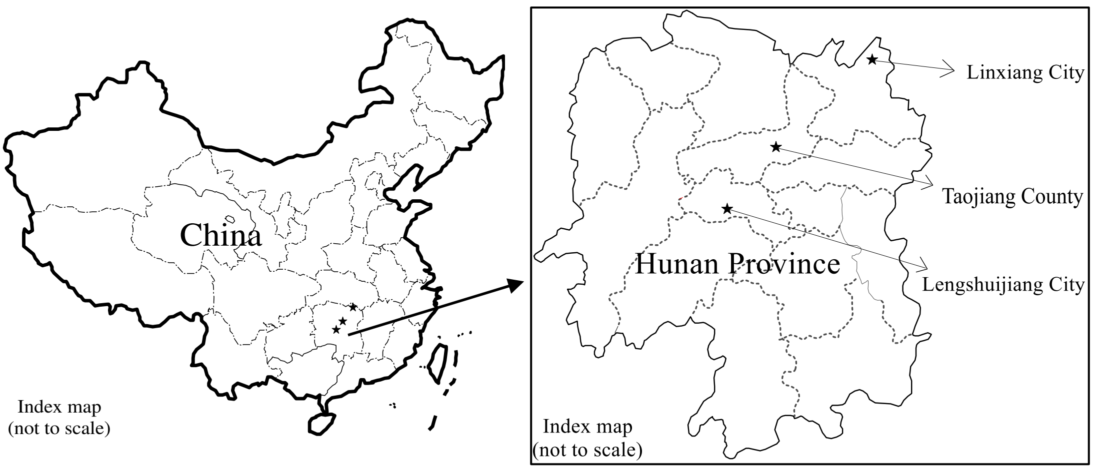

Figure 8 Map showing the locations of FSM application sites in Hunan Province. The three black stars indicate

the studied locations.

For the next study, we adopted TC150, advanced and intelligent equipment capable of measuring multi-frequencies. Figure 9 shows the field measurement photograph and relative results of the TC150 frequency selector in the karst exploration of a limestone mine in Linxiang City. The sampling frequencies are 36 within the range of 20 ~ 5000 Hz. The results show the noodles phenomenon possibly emerged by the static shift due to the presence of near-surface water-filled karst voids. The curve features of this pseudo section are similar to those of the theoretical finding (figure 6 vs figure 9b). Abnormal causes of FSM may possibly be attributed to the static shifts. For the direct evidence to prove the finding, the presence of these voids is varied by three drilling boreholes work. The drilling position is marked as YZ4, ZK2 and ZK1 in figure 9b. The drilling results are as follow. There was one karst cave filled with mud or clay under the YZ4 site along the depth of 36.0 m ~ 38.3 m. Two semi-filled karst caves were found under the ZK2 site with depth 22.5 ~ 31.0 m and 37.6 ~ 42.4 m respectively. The depth ranges of two caves found under the ZK1 site were 18.5 ~ 31.0 m and 34.5 ~ 40.5 m. The caves found by the drilling works indicate the presence of high water retaining and permeability of the underlying strata. Details can be accessed at Yang et al. (2020b).

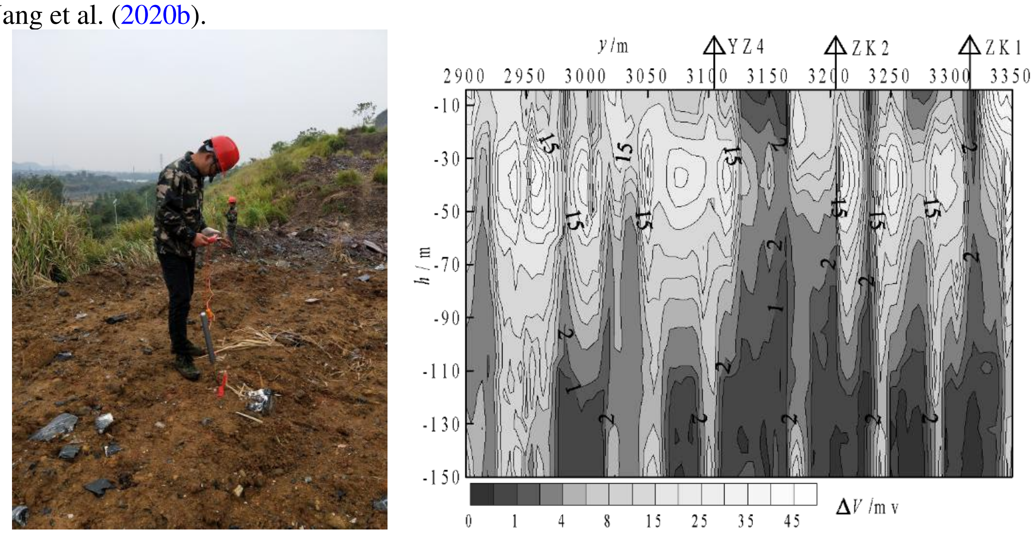

(a) (b)

Fig.9 (a) the photo of field measurement in Linxiang city; (b) and Pseudo section of the corresponding exploration result (Yang et al., 2020).

Figure 10 shows the results from the application of the TC300 frequency selector exploration for mineral water detection at a site (28°29′48"N, 112°3′21"E) in Taojiang county, Hunan province (Figure 8). Figure 10a are the plots of the profile curves of 20 frequencies, while the Figure 10b shows the potential difference ΔV pseudo section of 40 frequencies. The electrode spacing MN is 10 m and the station interval is 2 m in this case. The late Caledonian granodiorite was found exposed in the area. As study area is rural residential and there are transmission lines crossing therefore, the power of the lines was shut down at the time of data acquisition which inhibits the possible impacts of transmission lines on measurements.

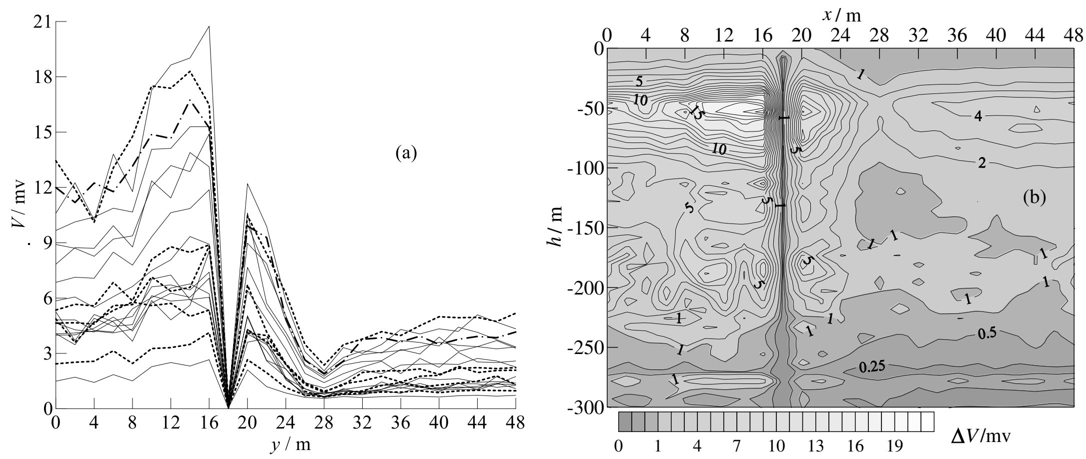

Figure 10 FSM application of mineral water exploration in Taojiang county, Hunan province. (a) Profile curves of potential difference ΔV; (b) seudo section of ΔV.

It can be seen from Figure 10a that a relatively very low potential anomaly occurred at 18th m of survey line, and the "noodles phenomenon" appears in Figure 10b, whose feature is similar with that of Figure 6d. Based on past experiences, this location can be marked as a potential site find water for groundwater exploration. However, according to the results of the site investigation, the anomaly is located just above an underdrain drainage channel of a small local reservoir (Figure 11). The channel can be divided into two parts, the rectangular ditch as a main part having dimensions as top buried depth 0.4 m, width 0.8 m and height 1 m, while the left side is a circular drainage pipe with about 0.3 m in diameter. The FSM anomaly at 18th m in Figure 10 is caused by the water semi-filled underdrain. Therefore, this field work further verified that the static shift is the main reason for the FSM anomaly.

Figure 11 An outcrop photo of underdrain

4 Summary

The present study applied MT two-dimensional finite element method to develop some theoretical insights into the causes of anomalies formulation in FSM, focusing on the study of TM polarization mode which is similar to the common field observation method of FSM. We calculated the profile curves and pseudo sections of the horizontal electric field component E_y along the direction of survey line based on the simulation of apparent resistivity ρ_s profile curves and pseudo sections. Results show obvious uplift in E_y profile curves with the increase in frequency in the Cartesian coordinate system in relation to the presence of near-surface low resistance abnormous, which is actually caused by the static shift phenomenon of MT. The pseudo-section of E_y also shows a significant static shift feature, it is similar to that of ρ_s, but with the isoline stretching in the opposite direction.

It is can be concluded from the two considered theoretical models that the static shift in the horizontal electric field component E_y profile curve generated by the natural electromagnetic field at the surface is an obvious phenomenon in the Cartesian coordinate system, but the relationship between the lifting direction of the profile curve and the frequency is opposite to that of the ρ_s profile curve.

Further, we discussed the measured results of FSM in karst exploration of limestone mines and the groundwater exploration in limestone and granite area, and analyzed the underground geology conditions, measured curves and pseudo sections. It is verified that the anomaly of FSM is naturally caused by the existence of inhomogeneous bodies in the near-surface zone. This demonstrates that the FSM, which has been applied in practice for about 40 years, actually uses the static shift phenomenon of the electromagnetic method. Therefore, the FSM method can be called the “static shift method”.

FSM is a passive source method, and its practical application is mainly concentrated in hydrogeology and engineering geology exploration within about 300 m depth. The field sources are not only homologous with MT but also possibly associated with surface humanistic electromagnetic signals to some extent. This article innovatively proposed the viewpoint of the “static shift method”, which only plays a role to start a further discussion on this issue. The effective utilization of static shift is like “turning waste into treasure”, which is expected to be further studied by more experts and scholars.

Acknowledgment

This study was supported by the National Natural Science Foundation of China [42074219] and the Natural Science Foundation of Hunan Province of China [12JJ3035].

References

Bao, G. S., Li, D. Q., Zhang, Y. S., et al. (1994). Research on the interfering electric field instrument. *The Chinese Journal of Nonferrous Metals*, *4*, 9-13.

Chen, L. S. (1981）. Improvements in the application of finite element method to the two dimensional forward solution in the magnetotelluric method. *Earth Science, 2*, 243-262.

Chen, X. B., Zhang, X., Hu, W. B. (2000). Application of finite-element direct iteration algorithm to MT 2-D forward computation OGP. *Progress in Geophysics, 35,* 487-496. DOI： 10.13810/j.cnki.issn.1000-7210.2000.04.011

Cheng, H., Bai, Y. C. (2014). Design and application of Audio frequency natural electric field instrument. *Progress in Geophysics, 29,* 2874-2879. DOI: 10.6038/pg20140658.

Coggon, J. H. (1971). Electromagnetic and electrical modeling by the finite element method. *Geophysics*, 36, 132-151.

Di, Q. Y.， Zhu, R. X., Xue, G. Q., et al. (2019). New development of the Electromagnetic (EM) methods for deep exploration. *Chinese Journal of Geophysics, 62*, 2128-2138. DOI: 10.6038/cjg2019M0633.

Farzamian, M., Alves Ribeiro, J., Khalil, M.A. et al. (2019). Application of Transient Electromagnetic and Audio-Magnetotelluric Methods for Imaging the Monte Real Aquifer in Portugal. *Pure and Applied Geophysics, 176*, 719–735. https://doi.org/10.1007/s00024-018-2030-7

Han, R. B., Wu, M. L. (1985). Application of frequency selection method of telluric current in engineering geology. *Geotechnical Investigation & Surveying, 13,* 76-79.

Han, R. B., Han, D. (2020). Theory and practice of frequency selection method for telluric electricity field. *Metallurgical industry press*, Beijing, China.

Hu, J. D., Wang, G. G., Chen, L. S., et al. (1982). Discussion on some problems in two-dimensional forward calculation of magnetotelluric field. *Oil Geophysical Prospecting, 17*, 47-55.

Hu, X. Y., Bi, B. T., Liu, G. X., et al. (2017). The lithospheric electrical structure of Ji'an-Fuzhou profile in the east part of South China. *Chinese Journal of Geophysics, 60*, 2756-2766. DOI: 10.6038/cjg20170721.

Huang, Z. H., Di, Q. Y., Hou, S. L. (2006). CSAMT static correction and its application. *Progress in Geophysics, 21*, 1290-1295.

Lei, D., Fayemi, B., Yang, L. Y., et al. (2017). The non-static effect of near-surface inhomogeneity on CSAMT data. *Journal of Applied Geophysics, 139*, 306-315.

Li, D. Q., He, J. S. (2021). A differential wide field electromagnetic method and its application in alkaline-surfactant-polymer (ASP) flooding monitoring. *Petroleum Exploration and Development, 48*: 693-701.

Liang, J., Wei, Q. F., Hong, J., et al. (2016). Application of self-potential method to explore water in karst area. *Geotechnical Investigation & Surveying, 44*, 68-78.

Lin, J. Q., Lei, C. S., Dong, Q. S. (1983). The natural low frequency electric field method. *Journal of Changchun University of Earth Sciences, 13*,114-126.

Liu, G. M., Ma, W., Liu, J. C., et al. (2018). Spatial domain topological processing technique for studying static effect in magnetotelluric sounding. *Geophysical and Geochemical Exploration, 42*,118-126.

Liu, J. X., Jiang, P. F., Tong, X. Z., et al. (2009). Application of BICGSTAB algorithm with incomplete LU decomposition preconditioning to two-dimensional magnetotelluric forward modeling. *Journal of Central South University (Science and Technology), 40*, 484-491.

Luo, H. F. (1994). The coal palaeoadit disaster and it's forecast by the natural electric field method. *The Chinese Journal of Geological Hazard and Control, 5(Suppl.)*, 277-284.

Singh, A., Ghosal, S., Agrahari, S. et al. (2022). Combined Electrical Resistivity and Time-Domain Induced Polarization Study for the Mapping of Heavy-Mineral-Enriched Placer Zones in Parts of Coastal Odisha, India. *Pure and Applied Geophysics, 179,* 1829–1841. https://doi.org/10.1007/s00024-022-03005-z

Song, W., Li, Z. T., Jin, Y., et al. (2021). Comprehensive application of hydrogeological survey and in-situ thermal response test. *Case Studies in Thermal Engineering, 2021, 27,* 101287. https://doi.org/10.1016/j.csite.2021.101287

Tournerie, B., Chouteau, M., Marcotte, D. (2007). Magnetotelluric static shift: Estimation and removal using the cokriging method. *Geophysics, 72*, F25-F34. DOI: 10.1190/1.2400625.

Xin, Y. S. (1982). Preliminary study on abnormal characteristics of audio geoelectric field method. *Journal of Shijiazhuang University of Economics, 5*, 44-53.

Xiong, B., Luo, T. Y., Chen, L. W., et al. (2021) Influence of complex topography on magnetotelluric-observed data using three-dimensional numerical simulation: A case from Guangxi area, China. *Applied Geophysics, 17*, 601-615. DOI: 10.1007/s11770-020-0842-6.

Xu, S. Z. (1994). Finite element method for geophysics. *Science Press,* Beijing, China.

Tan, H. D., Yu, Q. F., John, B., et al. (2003). Magnetotelluric three-dimensional modeling using the staggered-grid finite difference method. *Chinese Journal of Geophysics, 46,* 705-711.

Yang, D.M., Guo, W. B., Tan, Y., et al. (2019). Lithology and fissure characteristics of overburden in high-intensity mining. *Journal of China Coal Society, 44*, 786-795. doi: 10.13225/j.cnki.jccs.2018.6044

Yang, J. (1982). Experimental results and theoretical study of the stray current method in karst area. *Geophysical and Geochemical Exploration, 6*, 41-54.

Yang, T. C., He, J. S. (2013). Dispersion characteristics of Rayleigh waves in layered media. *Central South University Press,* Changsha, China.

Yang, T. C., Xia, D. L., Wang, Q. R., et al. (2017). Theoretical research and application of frequency selection method for telluric electricity field. *Central South University Press,* Changsha, China.

Yang, T. C., Chen, Z. C., Laing, J., et al. (2020a). Theoretical analysis of sounding anomaly and field application of the natural electric field frequency selection sounding method in groundwater exploration. *Earth Science Frontiers, 27*, 302-310. DOI: 10.13745/j.esf.sf.2020.6.34.

Yang, T. C., Wang, D. Q., Zhang, Y. P., et al. (2020b). Application research of comprehensive geophysical method to karst investigation in a productive mine. *Progress in Geophysics, 36*, 1145-1153. DOI: 10.6038/pg2021EE0275.

Zhou, F., Zhang, Z. Y., Tang, J. T., et al. (2021). 2.5-demension forward and inversion of WFEM in frequency domain. *Journal of Central South University (Science and Technology), 52*, 3273-3283. DOI: 10.11817/j.issn.1672-7207.2021.09.029

Zhou, H., Huang, C. L., Zhou, Y. W. (2009). Underground magneto fluid detector and its application in mine flood detection. *Mineral Engineering Research, 24*, 42-45.